

## Oxidation resistance and high-temperature mechanical properties of porous $\text{Si}_2\text{N}_2\text{O}/\text{Si}_3\text{N}_4$ composite ceramics

Liting Wei\* and Yangfang Wu

Department of Applied Chemistry, Yuncheng University, Yuncheng, 044000, PR China

$\text{Si}_2\text{N}_2\text{O}/\text{Si}_3\text{N}_4$  composite ceramics were prepared by pressureless sintered a  $\text{Si}_3\text{N}_4$  and  $\text{SiO}_2$  mixture with 2 mol%  $\text{Sm}_2\text{O}_3$ . The oxidation behavior and high-temperature strength of  $\text{Si}_2\text{N}_2\text{O}/\text{Si}_3\text{N}_4$  composite materials have been examined. The typical oxidation isotherm of  $\text{Si}_2\text{N}_2\text{O}/\text{Si}_3\text{N}_4$  ceramic is represented by an asymptotic law. The oxidation rate for  $\text{Si}_2\text{N}_2\text{O}/\text{Si}_3\text{N}_4$  was low as compared with those for  $\text{Si}_3\text{N}_4$  ceramic. Thin protective oxide scales formed after long exposures to air at 1400 °C and substantial crystallization of the intergranular glass phase with formation of  $\text{Sm}_{10}(\text{SiO}_4)_6\text{N}_2$  occurred during oxidation. Besides,  $\text{Si}_2\text{N}_2\text{O}/\text{Si}_3\text{N}_4$  composites showed excellent high-temperature strength like  $\text{Si}_3\text{N}_4$  ceramic and the residual strength ratio can be up to 80 % at 1100 °C which is much higher than  $\text{Si}_2\text{N}_2\text{O}$  single-phase ceramic. The degradation of strength at higher temperature results from the increase of intergranular glass phase due to diffusion of molecular oxygen.

**Key words:**  $\text{Si}_2\text{N}_2\text{O}/\text{Si}_3\text{N}_4$  composite ceramics, Oxidation resistance, High-temperature strength.

### Introduction

Wave transparent material is a kind of dielectric material which is used to protect radar system of aircraft and integrates multi-functions such as load bearing, wave transparent and heat-proofing. Silicon nitride ( $\text{Si}_3\text{N}_4$ ) ceramic is a suitable material for missile radome because of high mechanical strength, good resistance to ablation and good thermomechanical property [1, 2] and has received much attraction in the past decades. In particular, silicon oxynitride ( $\text{Si}_2\text{N}_2\text{O}$ ) ceramic with excellent oxidation resistance at severe conditions has gained much interest also [3, 4]. Consequently,  $\text{Si}_3\text{N}_4/\text{Si}_2\text{N}_2\text{O}$  composite ceramics is being studied to combine desirable properties such as oxidation resistance of  $\text{Si}_2\text{N}_2\text{O}$  and the strength of  $\text{Si}_3\text{N}_4$ .

Several researchers have demonstrated some potential properties of  $\text{Si}_3\text{N}_4/\text{Si}_2\text{N}_2\text{O}$  composites. Wen et al. [5] investigated the influences of rare-earth oxides on the mechanical properties of  $\text{Si}_2\text{N}_2\text{O}$  ceramics and indicated that the samples doped with  $\text{La}_2\text{O}_3$  and  $\text{Sm}_2\text{O}_3$  with elongated crystals exhibit higher flexural strength. Subsequently, Wei et al. [6] prepared  $\text{Sm}_2\text{O}_3$ -doped  $\text{Si}_3\text{N}_4/\text{Si}_2\text{N}_2\text{O}$  composite ceramics with excellent thermal shock resistance and dielectric properties. Jia et al. [7] fabricated  $\text{Si}_3\text{N}_4/\text{Si}_2\text{N}_2\text{O}$  composite material by silicon sol infiltration of aqueous gelcasting prefabricated  $\text{Si}_3\text{N}_4$  green compact

with a moderate dielectric constant of 4.0-5.0 (at 21-39 GHz). Pei et al. [8] evaluated that  $\text{Si}_3\text{N}_4/\text{Si}_2\text{N}_2\text{O}$  composites which were prepared with in situ liquid pressureless sintering process using  $\text{Yb}_2\text{O}_3$  and  $\text{Al}_2\text{O}_3$  powders as sintering additives by gelcasting showed no macroscopic cracks and the critical temperature difference ( $\Delta T_c$ ) could be up to 1400 °C. However, the oxidation resistance and high-temperature strength of  $\text{Si}_3\text{N}_4/\text{Si}_2\text{N}_2\text{O}$  have not been carried out yet. Therefore,  $\text{Si}_2\text{N}_2\text{O}/\text{Si}_3\text{N}_4$  composite ceramics were fabricated by gas pressure sintering using  $\text{Sm}_2\text{O}_3$  powders as sintering additives in the present work. Oxidation behavior and the high-temperature strength of  $\text{Si}_2\text{N}_2\text{O}/\text{Si}_3\text{N}_4$  composite ceramics as well as  $\text{Si}_2\text{N}_2\text{O}$ ,  $\text{Si}_3\text{N}_4$  single-phase ceramics were investigated.

### Materials and Experimental Procedure

$\alpha$ - $\text{Si}_3\text{N}_4$  (purity = 99.99 %,  $D_{50} \leq 0.7 \mu\text{m}$ ),  $\text{SiO}_2$  (purity = 99.9 %,  $D_{50} \leq 1.0 \mu\text{m}$ ) and  $\text{Sm}_2\text{O}_3$  powders (99.9 % pure) were used as starting powders. The molar contents of  $\text{Si}_3\text{N}_4$ ,  $\text{SiO}_2$  and  $\text{Sm}_2\text{O}_3$  were modified and listed in Table 1 in order to prepare the  $\text{Si}_2\text{N}_2\text{O}/\text{Si}_3\text{N}_4$  composites with various  $\beta$ - $\text{Si}_3\text{N}_4$  contents. Samples were given brief names, for example, as-prepared samples with  $\text{SiO}_2 + 2 \text{ mol}\% \text{Sm}_2\text{O}_3 + 60 \text{ mol}\% \text{Si}_3\text{N}_4$  as starting materials were designated as SN60. The above starting powders according to a certain ratio shown in Table 1 were weighed and wet mixed in anhydrous alcohol in a plastic bottle, and then the mixture was milled with high-purity  $\text{Si}_3\text{N}_4$  balls for 12 h. After milling, the slurry was dried, sieved, and bilaterally pressed to form rectangular bars at 100 MPa.

\*Corresponding author:  
Tel : +86-15103485027  
Fax: +86-03592090378  
E-mail: weiliting\_job@163.com

The green bodies of SN50, SN60 and SN70 were placed in a graphite crucible and sintered for 2 h at 1750 °C and SN100 for 2 h at 1800 °C, respectively.

The porosity of as-prepared samples was measured by the Archimedes method. The three-point bending strength was measured at room temperature to 1400 °C on rectangular bars (3 mm × 4 mm × 20 mm) at a crosshead speed of 0.5 mm/min by an instrument (Instron 1195, Instron Co., Buckinghamshire, England). Each final value was averaged over five measurements. Young's modulus  $E$  was measured by pulse echo overlap method in the frequency range from 2 to 10MHz with cylindrical specimens (20 mm diameter and 16mm thick) and it can be calculated according to the equation:

$$E = \rho \times \left( C_L^2 - \frac{4}{3} \times C_S^2 \right) \quad (1)$$

where  $\rho$  is density of the sample,  $C_L$  and  $C_S$  are the speed of transverse wave and longitudinal wave, respectively. Oxidation experiments were performed in a furnace equipped with SiC heating elements at 1400 °C. Sample size was the same as that for bending strength tests. The samples were weighed after the test at each time, using a balance with the accuracy of 0.01 mg.

Phase composition was determined by X-ray diffractometry (Model X'Pert PRO, PANalytical, Ltd., Holland). The quantitative phase analyses were performed by comparing the peak intensity ratios. The microstructures of bulk samples were observed by scanning electron microscope (Model JSM-7000F, JEOL, Japan). Energy-dispersive X-ray spectroscopy (EDS) was used for chemical analysis of intergranular phases.

## Results and Discussion

### Phase, microstructure and mechanical performance

SiO<sub>2</sub>, 2 mol% Sm<sub>2</sub>O<sub>3</sub> and different molar ratio of  $\alpha$ -Si<sub>3</sub>N<sub>4</sub> and SiO<sub>2</sub> as starting materials were sintered for 2 h at 1750 °C under 0.5MPa nitrogen pressure to prepare Si<sub>2</sub>N<sub>2</sub>O/Si<sub>3</sub>N<sub>4</sub> composites. The XRD patterns of the as-sintered samples are presented in Fig. 1. The diffractograms show that only peaks of Si<sub>2</sub>N<sub>2</sub>O are detected in sample SN50 and no peak for other crystalline phases are detected, which suggests complete reaction of  $\alpha$ -Si<sub>3</sub>N<sub>4</sub> and SiO<sub>2</sub> after sintering at 1750°C. The formation of Si<sub>2</sub>N<sub>2</sub>O can be illustrated as the following reaction<sup>[9]</sup>:



It can be seen that the sample SN60 and SN70 are well crystallized and only  $\beta$ -Si<sub>3</sub>N<sub>4</sub> and Si<sub>2</sub>N<sub>2</sub>O are identified. Quantitative analysis (as shown in Table 1) indicates that the content of  $\beta$ -Si<sub>3</sub>N<sub>4</sub> increases with the

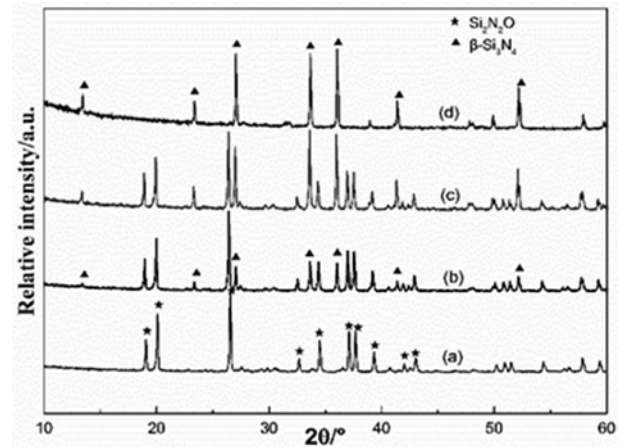


**Fig. 1.** X-ray diffraction of as-sintered samples (a) SN50, (b) SN60, (c) SN70, (d) SN100.

**Table 1.** The molar ratio of composition in starting materials and the  $\beta$ -Si<sub>3</sub>N<sub>4</sub> contents in as-sintered samples.

Materials	The molar ratio of composition in starting materials (mol. %)			The calculated contents of $\beta$ -Si <sub>3</sub> N <sub>4</sub> (mol. %)	
	Sm <sub>2</sub> O <sub>3</sub>	Si <sub>3</sub> N <sub>4</sub>	SiO <sub>2</sub>	Theoretical content	True content
SN50	2	49	49	0	0
SN60	2	60	38	37	27
SN70	2	70	28	60	41
SN100	2	98	0	100	100

increasing  $\alpha$ -Si<sub>3</sub>N<sub>4</sub> content in starting materials. The true content of  $\beta$ -Si<sub>3</sub>N<sub>4</sub> lower than theoretical content indicates surface oxygen of  $\alpha$ -Si<sub>3</sub>N<sub>4</sub> involved in the reaction.

The microstructure of Si<sub>2</sub>N<sub>2</sub>O/Si<sub>3</sub>N<sub>4</sub> composite is presented in Fig. 2. Lath-like silicon oxynitride grains and a mass of intergranular glassy phase are developed in SN50 samples. Sample SN60 exhibits plate-like grains overlapped with rod-like grains. Increasing Si<sub>3</sub>N<sub>4</sub> content results in more rod-like grains in the morphology which are not sufficiently developed because of high-viscosity liquid phase formed during liquid-phase sintering as shown in Fig. 2(c). Sample SN100 shows well-developed rod crystals.

Properties of the obtained samples are listed in Table 2. Porosity of the samples increases with increasing  $\alpha$ -Si<sub>3</sub>N<sub>4</sub> content, because excess  $\alpha$ -Si<sub>3</sub>N<sub>4</sub> tends to develop into rod-shaped grains, among which reciprocal overlap joint results in high porosity. As indicated, the strength and Young's modulus decrease with the increasing porosity of the samples.

### Oxidation resistance

Fig. 3(a) shows the oxidation curves of Si<sub>2</sub>N<sub>2</sub>O/Si<sub>3</sub>N<sub>4</sub> composite ceramics with different contents of Si<sub>3</sub>N<sub>4</sub> at 1400 °C. It can be noted from the Fig. 3 that the weight gain percentage tends to go up gradually with the

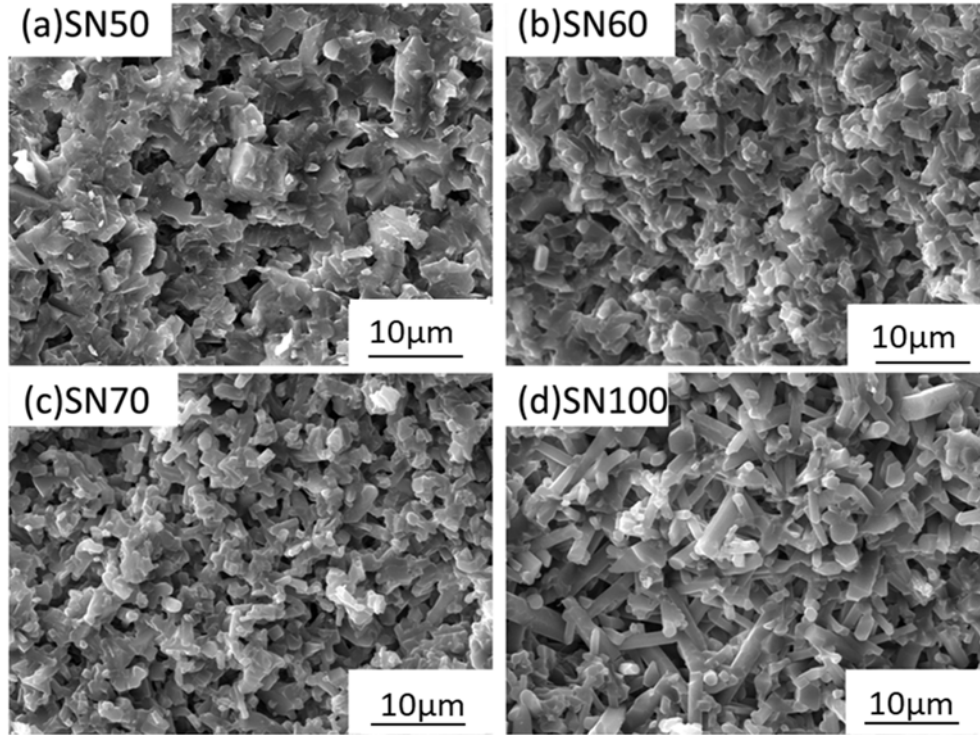
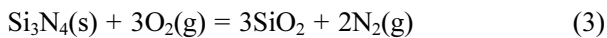


**Fig. 2.** SEM for the as-sintered samples (a) SN50, (b) SN60, (c) SN70, (d) SN100.

**Table 2.** Properties of as-sintered samples with different contents of  $\beta$ - $\text{Si}_3\text{N}_4$ .

Sample	Porosity/%	Flexural strength /MPa	Young's modulus /GPa
SN50	14.7	357±11	215±4
SN60	19	288±10	192±5
SN70	28.7	223±22	175±7
SN100	20.3	354±20	287±3

increasing content of  $\text{Si}_3\text{N}_4$  phase at the same oxidation time, which is mainly related to the phase content and porosity of the samples. On one hand, as the content of  $\text{Si}_3\text{N}_4$  increases, the porosity increases gradually, making oxygen more easily diffused into the interior. On the other hand, passive oxidation occurs when the partial pressure of oxygen is greater than the partial pressure of  $\text{SiO}$  gas [10], so the samples will be oxidized by the following two equations:



It can also be seen from the equation that the weight gain percentage of silicon nitride is greater than that of  $\text{Si}_2\text{N}_2\text{O}$ . Therefore, the mass gain percentage is gradually increasing with the increasing content of  $\text{Si}_3\text{N}_4$ . Sample SN50 after oxidized for 5 h has slight weight loss, which possibly results from volatilization of liquid phase at high temperature.

When oxidized at a higher temperature (1400 °C), it

can be found that the mass change curve deviates from the parabolic fit curve, and Evans [11] suggests that it can be represented by an asymptote treatment of the oxidation isotherms [Eq. (5)] and formulated an asymptotic equation for the case of self-blocking pores, the rate of oxygen uptake being determined by the number of pores still remaining open.

$$\frac{\Delta m}{m} = \frac{\Delta m_a}{m} (1 - e^{-k_a t}) \quad (5)$$

$\Delta m_e$  represents the final mass gain when the horizontal region of the oxidation isotherm is reached; the asymptotic rate coefficient  $k_a$  represents a “time constant” to reach this region. When all pores have been closed there still exists slow oxidation at the geometrical surface, so  $\Delta m/m$  can't exceed  $\Delta m_a/m$ . For practical purposes this can be neglected compared with the very high initial oxidation rate. Equation 5 can be rewritten in the form:

$$\ln\left(1 - \frac{\Delta m}{\Delta m_a}\right) = -k_a t \quad (6)$$

Fig. 3(b) gives the asymptotic plots for sample SN60 and SN100 with the similar porosity and the results of the asymptotic treatment of both materials are collected in Table 3. The time  $t_{99}$ , 99 % of the final mass gain is reached, calculated with Eq. (6) using the measured values. It is indicated that  $\text{Si}_3\text{N}_4$  is more easily oxidized in air to form amorphous  $\text{SiO}_2$ , which reduces the open

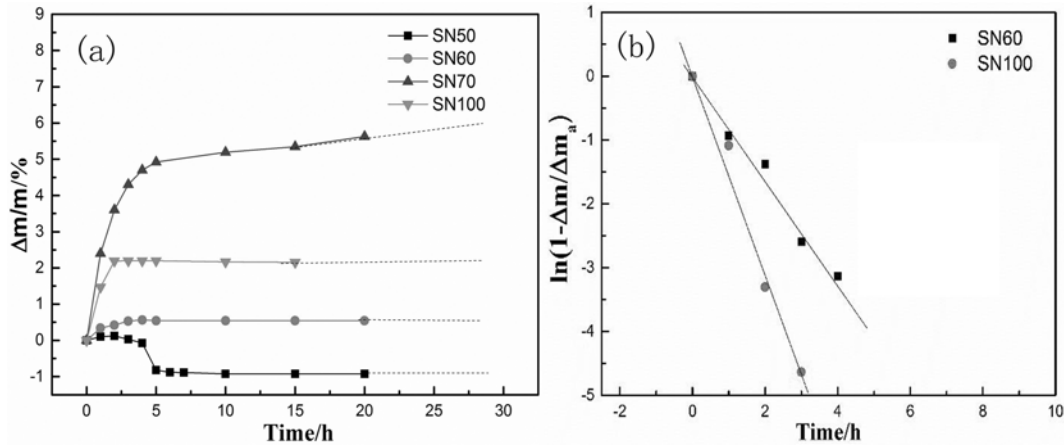


**Fig. 3.** (a) Mass gain of samples oxidized in dry air at 1400 °C (b) Asymptotic plot of the oxidation isotherms of SN60 and SN100.

**Table 3.** Results of the asymptotic treatment of the oxidation isotherms of SN60 and SN100.

sample	porosity/%	$\frac{\Delta m_a}{m}$ /%	$k_d/\text{h}^{-1}$	Time $t_{99}$ ( $\frac{\Delta m/m}{\Delta m_a/m} = 0.99$ )/h
SN60	19	0.7	0.82	5~7
SN100	20	2.3	1.6	3~4

porosity and reaches the maximum mass increase in a shorter time. The  $\text{Si}_2\text{N}_2\text{O}$  sample exhibited better oxidation resistance than  $\text{Si}_3\text{N}_4$ .

Fig. 4(a) (b) shows the XRD patterns of SN60 and SN100 oxidized at 1400 °C for different hours. After oxidation for 2 h, the peak of  $\text{Si}_2\text{N}_2\text{O}$  phase of SN60 decreased slightly, while the peak of  $\beta\text{-Si}_3\text{N}_4$  phase of SN100 significantly reduced. It suggests that  $\text{Si}_2\text{N}_2\text{O}/\text{Si}_3\text{N}_4$  composites have the better oxidation resistance than  $\text{Si}_3\text{N}_4$ . Besides, crystalline  $\text{Sm}_{10}(\text{SiO}_4)_6\text{N}_2$  and cristobalite ( $\text{SiO}_2$ ) also occurred after oxidation for 2 h in SN60. This phenomenon is also observed in sintered  $\beta\text{-Si}_3\text{N}_4$  material (SN100). It is considered to result from a ‘reaction-couple’ established between the amorphous oxide scale and the amorphous intergranular phase [12, 13]. The reaction-couple operates to decrease the chemical gradient between the two phases. As observed in the present work the outward diffusion of cations (Sm) to the external oxide layer results in the formation of mixed scaled from which  $\text{Sm}_{10}(\text{SiO}_4)_6\text{N}_2$  crystals nucleate and grow. Fig. 4 exhibits SEM fracture photographs of samples oxidized at 1400 °C for 30 h. The uniform and dense oxide layer appeared and the thickness of the

surface scale was about 7.5  $\mu\text{m}$  and 9.7  $\mu\text{m}$  for SN60 and SN100, respectively, which can inhibit molecular oxygen from entering the interior of the material, thereby hindering further oxidation. The microstructures of the samples at the center are shown in Fig. 4(e), (f). Compared with the sample before oxidation (Fig. 2(b), (d)), the intergranular amorphous phase of SN100 increases obviously. The degree of oxidation at the center of the porous  $\beta\text{-Si}_3\text{N}_4$  ceramic is more serious than that of the  $\text{Si}_2\text{N}_2\text{O}/\text{Si}_3\text{N}_4$  composite ceramic with the same oxidation time.

Table 4 compares the properties of  $\text{Si}_2\text{N}_2\text{O}/\text{Si}_3\text{N}_4$  with other structural/functional ceramics [14, 15]. The results demonstrate that the oxidation resistance of  $\text{Si}_2\text{N}_2\text{O}/\text{Si}_3\text{N}_4$  composite with 2 mol%  $\text{Sm}_2\text{O}_3$  are superior to those of  $\text{Si}_3\text{N}_4$  ceramics and  $\text{Si}_2\text{N}_2\text{O}$  ceramics with other metal oxide additive.

#### High-temperature strength of $\text{Si}_2\text{N}_2\text{O}/\text{Si}_3\text{N}_4$ composites

Temperature dependence of flexural strength of the  $\text{Si}_2\text{N}_2\text{O}/\text{Si}_3\text{N}_4$  composite ceramic with  $\text{Si}_2\text{N}_2\text{O}$ ,  $\text{Si}_3\text{N}_4$  single-phase ceramic was influenced by the difference in properties of the intergranular phase (Fig. 5). The residual strength of SN50 showed a sharp decline and slight plastic deformation occurred at 800 °C. It is suggested that the degradation of strength results from the low softening temperature of the intergranular amorphous phase produced by the reaction of plenty of  $\text{SiO}_2$  and  $\text{Sm}_2\text{O}_3$ .

The strength in SN60, SN70 and SN100 remained almost steady from 800~1000 °C and fell slightly to 1100°C. At temperatures >1000 °C, oxidation probably

**Table 4.** Selected properties of several structural/functional ceramics.

Properties	$\text{Si}_2\text{N}_2\text{O}/\text{Si}_3\text{N}_4$ (2 mol% $\text{Sm}_2\text{O}_3$ )	$\text{Si}_3\text{N}_4$ (2 mol% $\text{Sm}_2\text{O}_3$ )	$\text{Si}_2\text{N}_2\text{O}$ (1 mol% $\text{Sm}_2\text{O}_3$ )	$\text{Si}_2\text{N}_2\text{O}$ (10 wt% $\text{Y}_2\text{O}_3$ and 6 wt% $\text{Al}_2\text{O}_3$ )
Porosity (%)	19	20	21	10
Weight gain (%)	0.7	2.3	0.6	2.6
Reference	This work	This work	Reference [14]	Reference [15]

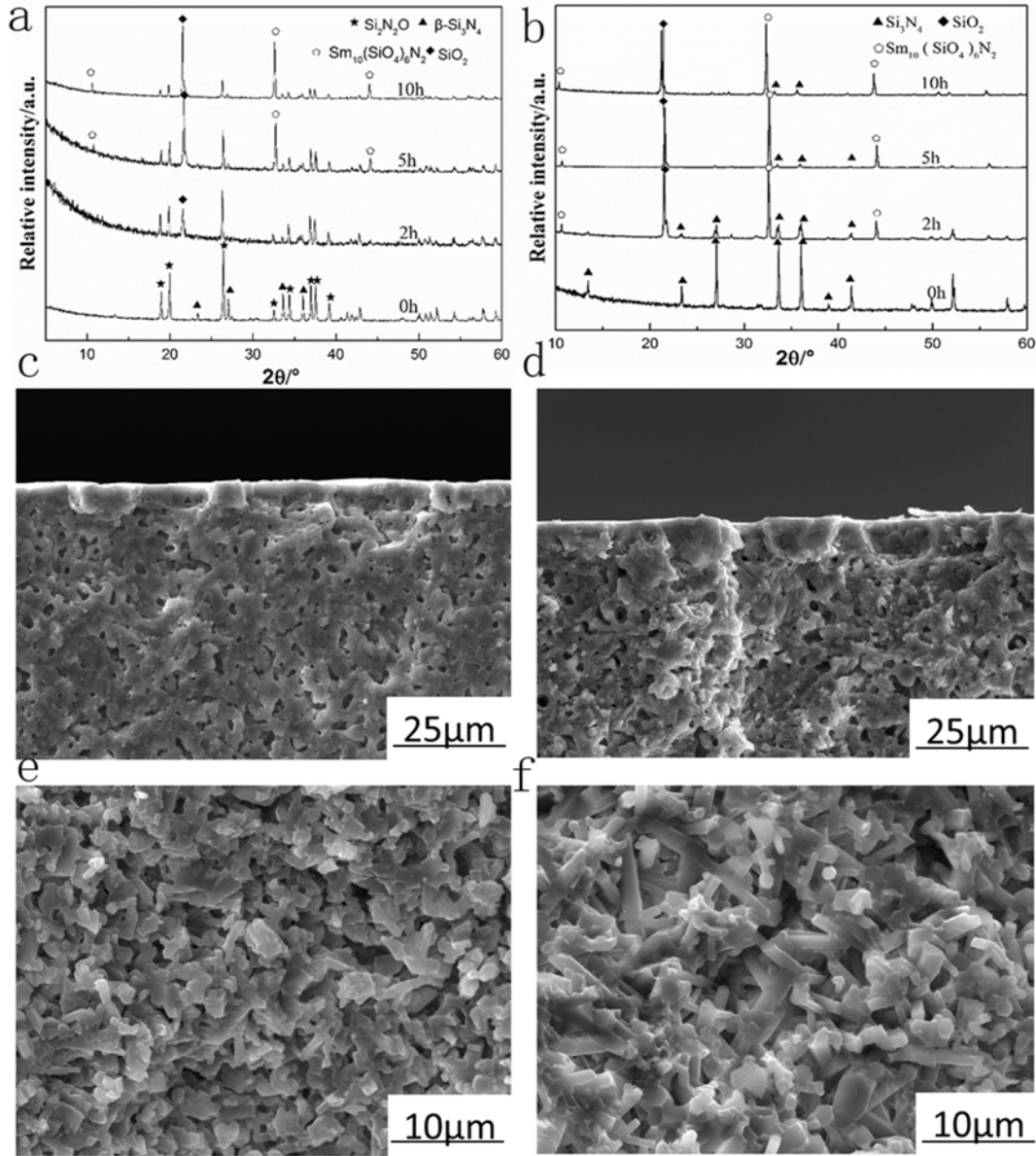


**Fig. 4.** (a)(b) XRD patterns of surface of SN60 and SN100 after oxidation for different times Fig. 6(c, d, e, f) SEM fracture photographs of samples oxidized at 1400 °C for 30 h (c) SN60, at surface (e) SN60, at center part (d) SN100, at surface (f) SN100, at center part.

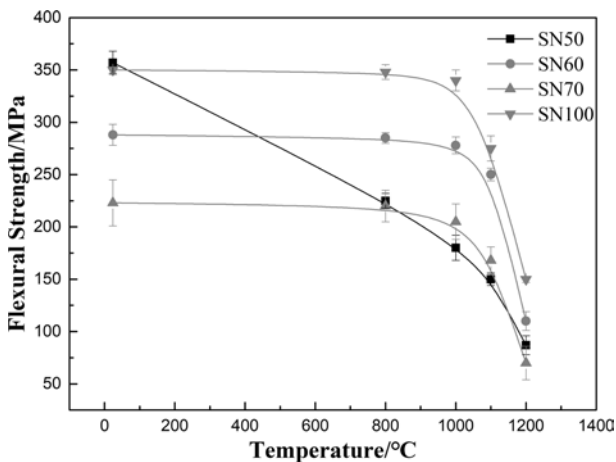


**Fig. 5.** Temperature dependence of flexural strength of samples.

played an important role. The generation and softening of the intergranular vitreous phase induced the decrease of strength. The strength of the three samples above fell sharply up at 1200 °C. As illustrated in Fig. 6, the content of the glass phase increased with the rising of temperature. EDS analysis on the A, B, C, and D regions (intergranular phase regions) of Fig. 6 were performed. In order to ensure the accuracy of the oxygen content comparison, the areas in the figure are 1 ± 0.3 mm from the sample surface. Table 5 is EDS analysis of A, B, C and D regions. It can be seen that the oxygen content was significantly increased from 1100 °C and getting much higher at 1200 °C. The flexural strength of SN60 at higher temperature under air atmosphere decreased remarkably, which is mainly ascribed by diffusion of molecular oxygen. As the

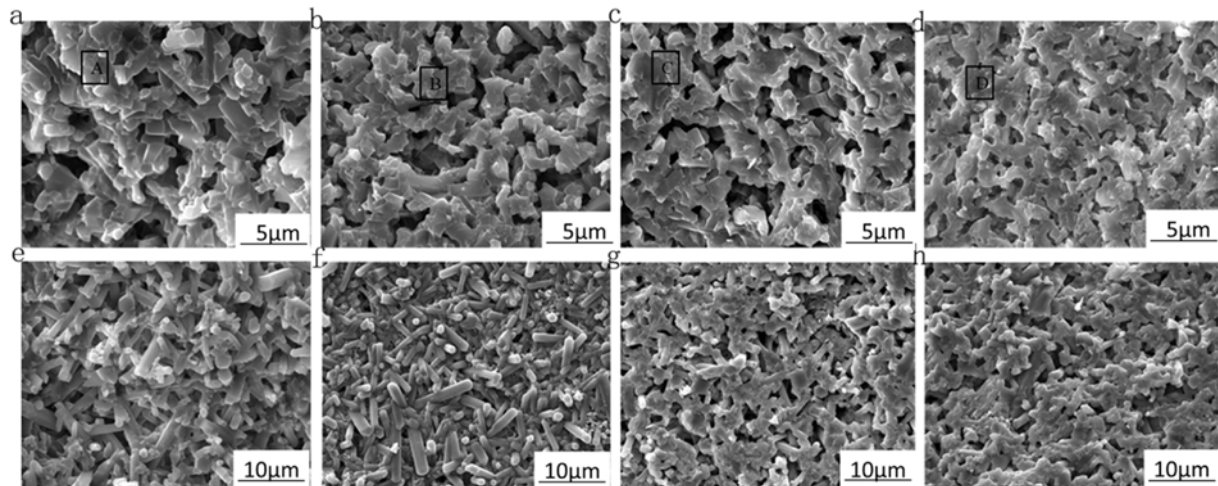


**Fig. 6.** Fracture morphology of SN60 and SN100 at different temperatures (a)(e) room temperature (b)(f) 1000 °C (c)(g) 1100 °C (d)(h) 1200 °C, respectively

**Table 5.** EDS spectrum analysis on the A, B, C, and D regions of Fig. 6 (SN60).

Element	A		B		C		D	
	wt.%	at.%	wt.%	at.%	wt.%	at.%	wt.%	at.%
N K	13.08	21.72	22.15	34.68	28.69	40.45	26.16	35.90
O K	15.32	21.98	16.19	22.78	20.74	25.60	29.39	35.32
Si K	68.30	55.80	57.65	41.92	47.75	33.58	41.50	28.40
Sm L	3.30	0.50	4.00	0.62	2.81	0.37	2.95	0.38

temperature increased, the content of intergranular vitreous phase increased, which induces softening.

### Conclusions

In this study,  $\text{Si}_2\text{N}_2\text{O}/\text{Si}_3\text{N}_4$  composite ceramics with excellent performance of oxidation resistance and high-temperature strength was prepared by gas pressure sintering. The typical oxidation isotherm of  $\text{Si}_2\text{N}_2\text{O}/\text{Si}_3\text{N}_4$  ceramic is represented by an asymptotic law. The oxidation rate for  $\text{Si}_2\text{N}_2\text{O}/\text{Si}_3\text{N}_4$  was low as compared with those for  $\text{Si}_3\text{N}_4$  ceramic. The flexural strength of  $\text{Si}_2\text{N}_2\text{O}/\text{Si}_3\text{N}_4$  composites with  $\text{Si}_3\text{N}_4$  ceramic remained steady up to 1000 °C, while the strength of  $\text{Si}_2\text{N}_2\text{O}$  ceramics fell sharply at 800 °C because of the low softening temperature of the residual intergranular glassy phase. So we can get  $\text{Si}_2\text{N}_2\text{O}/\text{Si}_3\text{N}_4$  composite ceramic with excellent overall performance of strength and oxidation resistance.

### Acknowledgments

The authors are thankful for the financial support provided by the Science and Technology Research Project of Yuncheng University, China (CY-2017009).

### References

1. F.-L. Riley, *J. Am. Ceram. Soc.* 83 (2000) 245-265.
2. K.-S. Mazdiyasi, and R. Ruh, *J. Am. Ceram. Soc.* 64 (1981) 415-419.
3. M. Radwan, T. Kashiwagi, and Y. Miyamoto, *J. Eur. Ceram. Soc.* 23 (2003) 2337-2341.
4. R.-J. Xie, M. Mitomo, F.-F. Xu, G.-D. Zhan, B. Yoshio and A. Yoshio, *J. Eur. Ceram. Soc.* 22 (2002) 963-971.
5. J.-B. Wen, H.-J. Wang, L. Fan, L.-T. Wei, M. Niu, H.-F. Gao and Z.-X. Cai, *J. Am. Ceram. Soc.* 102[1] (2019) 136-143.
6. L.-T. Wei, Y.-H. Yu, and J. Jiao, *J. Ceram. Process. Res.* 19[2] (2018) 126-129.
7. D.-C. Jia, Y.-F. Shao, B.-Y. Liu, and Y. Zhou, *Mater. Chem. Phys.* 124 (2010) 97-101.
8. Y.-C. Pei, S.-Q. Li, C.-Q. Yu, Z.-Y. Huang, J.-T. Ma, and J.-L. Li, *Ceram. Int.* 35 (2009) 3365-3369.
9. M. Ohashi, K. Nakamura, K. Hirao, M. Toriyama, and S. Kanzaki, *Ceram. Int.* 23 (1997) 27-37.
10. S.-C. Singhal, *J. Mater. Sci.* 11[3] (1976) 500-509.
11. F. Porz and F. Thummler, *J. Mater. Sci.* 19[4] (1984) 1283-1295.
12. D. -R. Clarke and F. -F. Lange, *J. Am. Ceram. Soc.*, 63 (1980) 586-589.
13. D.-R. Clarke, In *Progress in Nitrogen Ceramics*, ed. F. L. Riley. Martinus Nijhoff, The Hague, 1983, p. 421.
14. L.-T. Wei, J.-B. Wen, L. Fan and H.-J. Wang, *J. Chin. Ceram. Soc.* 46[6] (2018) 780-784.
15. C. O'Meara, J. Sjöberg and G. Dunlop, *J. Eur. Ceram. Soc.* 7 (1991) 369-378.